IMPACT ANALYSIS OF A CONCRETE STORAGE CONTAINER

H.P. Lee

Ontario Hydro
700 University Avenue
Toronto, Ontario, Canada

ABSTRACT

A concrete container with impact limiters is analyzed for a 9m free drop to a rigid ground. The complete finite element model is built using MSC/PATRAN. Analysis is then carried out using DYNA3D. Results are again completely processed using MSC/PATRAN in terms of time history plots of energy, momentum and contact force; deformation of the container during impact; and stress/strain distribution in the container at different times.

1. INTRODUCTION

This paper illustrates an impact analysis of a concrete container experiencing a 9m free drop to a rigid ground. The container with payload is protected by impact limiters at its top and bottom ends. The drop orientation is assumed to be an upside-down corner drop with its center of gravity directly above the initial impact point. The MSC/PATRAN is used for pre- and post-processing while the analysis is conducted using DYNA3D. The paper reports the geometrical/material modelling, analysis, impact response and damage in terms of energy, momentum, contact force, stresses, strains and deformation.

2. GEOMETRY OF THE CONTAINER SYSTEM

The complete container structural system is composed of three major items: the container itself, the impact limiter No. 1 and the impact limiter No. 2.

Fig. 1 provides a section and a plane view of the container. It is a thick rectangular concrete tank with a lid at the top. The height of the tank and the thickness of the lid are 3.002m and 0.480m respectively which result in the complete container with a total height of 3.482 m. The tank has an outside dimension of 2.110 m x 2.418 m and an inside dimension of 1.012 m x 1.320 m. Both outside and inside of the container, as well as the lid itself, are enclosed by a 12 mm steel plate. Within the enclosed plates, both the tank and the lid are filled with high density concrete. The lid is finally seal-welded to the tank along their corresponding circumferences.

Impact limiter No. 1 (Fig. 2) is defined as the limiter covering the lid end of the container. It is basically a rectangular hollow structure sheathed by 304L stainless steel and filled with rigid polyurethane foam to absorb impact energy. The portion to directly protect the lid is enclosed by 10 mm thick horizontal plates and 5 mm thick vertical plates all around with 1.005 m in height. There is a 1.0 m x 10 m x 0.5 m cubic cavity in the centre. This portion of the limiter is filled with 15 lb/ft^3 density rigid foam. The projected portion is designed to protect the sides of the container. The outer skin is composed of 5 mm thick plates while the inner skin of 5 mm plates on two opposite sides and 10 mm plates on the other two opposite sides. The projected height is 1.215 m which leads the total height of the impact limiter No. 1 to 2.220 m. This portion is filled with 17 lbs/ft^3 density foam.

Impact limiter No. 2(Fig. 2) is defined as the limiter covering the other end (bottom end) of the container. This limiter is identical to impact limiter No. 1 except that the projected height to protect the sides of the container is reduced to 0.615 m which results in the total height of the limiter being 1.620 m.

3. MATERIAL PROPERTIES

There are four different types of material involved: 1) the structural carbon steel for the container liners, 2) the 304L stainless steel for the impact limiter skin, 3) the container high density concrete, and 4) the rigid polyurethane foam which fills the impact limiters. The rigid foam is further divided into two types of 17 lbs/ft^3 and 15 lbs/ft^3 density respectively. Their mechanical properties are reported in the following:

3.1 Steel Liners

The steel liners are made of the Canadian Standard G40.21M 300 WT steel whose stress-strain curve based on the tensile test on a specimen is shown in Fig. 3. Linear strain hardening is assumed in this case in order to fit to the input format of the computer program. Judging the container may not experience significant plastic strain because it is protected by the impact limiter, it is decided that the linear approximation should resemble closer to the earlier stage of the post-yielding curve. The used properties are:

Density	$r = 7{,}850$ kg/m^3
Young's Modulus:	$E = 203 \times 10^3$ MPa
Poisson's Ratio:	$n = 0.3$
Initial Yield Strength:	$s_y = 370$ MPa
Hardening Modulus:	$E_t = 1.5 \times 10^3$ MPa

3.2 304L Stainless Steel

A typical stress-strain curve based on Ref. 1 is shown in Fig. 4 and indicates an almost linear strain hardening up to its final ductile fracture failure. The mechanical properties employed in the analysis are:

Density	$r = 8{,}027$ kg/m^3
Young's Modulus:	$E = 193 \times 10^3$ MPa
Poisson's Ratio:	$n = 0.28$
Initial Yield Strength:	$s_y = 305$ MPa
Hardening Modulus:	$E_t = 1.25 \times 10^3$ MPa

3.3 Concrete

The concrete used for the container is a specially designed high density mix. The compression and tension tests from Ref. 2 form the basis for constructing the two needed constitutive laws of the yield model and the equation of state, as well as the following generic properties required for computer input:

Density:	$r = 3535$ kg/m$_3$
Shear Modulus:	$G = 20 \times 10^3$ MPa
Cutoff Pressure:	$P_{min} = 1.4$ MPa

On the yield model, the strength of concrete is based on the Mohr-Coulomb failure criteria and expressed as a function of hydrostatic pressure which represents the mean normal stress in a multi-stress state. This relation identifies that the strength depends on the confined pressure, the higher the confined pressure the greater the compressive strength. The final curve with the shape of an inverse polynomial function is generated as shown in Fig. 5.

The equation of state is shown in Fig. 6 relating hydrostatic pressure to the volume change. Due to lack of experimental data on equation of state for concrete, a simplified segmentally linearized relationships is assumed after consulting Ref. 3. If the pressure is released after concrete being crushed (i.e. beyond point A in Fig. 7), elastic unloading is considered with permanent volume change. If the concrete is subjected to tension, the required negative pressure to increase the volume is similar to that of compression with the same bulk modulus. This continues until the maximum tensile strength of the concrete as represented by the spall limit P_{min} is reached. Then the concrete starts to crack and pressure is dropped to zero.

3.4 Rigid Polyurethane Foam

Two types of foam identified as 17 lbs/ft^3 and 15 lbs/ft^3 are filled into different portion of the impact limiter (see Fig. 2). At the time of analysis, mechanical properties for these two foams are not available. By treating properties as functions of density (Ref. 4), a previous known foam with the density of 23 lbs/ft^3 is adopted and modified in accordance with the following formula:

$$\text{Property} = A\,(\text{Density})^B \qquad (1)$$

where A and B are parameters varied for different types of properties. The resulting generic properties for computer input are:

Foam type #1 (17 lbs/ft^3 density)	
Density	r = 272 kg/m3
Shear Modulus:	G = 54.1 MPa
Cutoff Pressure	P_{min} = 1.3 MPa
Foam type #2 (15 lbs/ft^3 density)	
Density	r = 240 kg/m3
Shear Modulus:	G = 47.4 MPa
Cutoff Pressure	P_{min} = 1.124 MPa

Similar to concrete, two constitutive laws of the yield model and the equation of state are required for the foams. The previous test data of 23 lbs/ft^3 density foam were adopted again and modified in accordance with Eq. 1 to generate yield models as shown in Fig. 7. The equation of state possesses a unique test yet to be carried out. A curve based on engineer's judgement is assumed for the current analysis as shown in Fig. 8. The difference between the two foams was ignored.

4. FINITE ELEMENT MODELLING

The container structural system is transformed into a mathematical model using MSC/PATRAN(Ref. 5). The steel liners and the impact limiter stainless steel skins are simulated by four-nodes shell elements while the concrete, the rigid polyurethane foam, the payload and the rigid ground by eight-nodes solids. MSC/PATRAN, functioning as a pre-processor, creates these elements and generates a set of input data for later analyses. Because the configuration of the system is rectangular in shape and hence lost its advantage of symmetry, the entire structure of the container system is modelled.

Fig. 9a illustrates the shell elements in wire frame simulating steel liners and limiter skins of the system and its relative position against the target pad. Similarly, Fig. 9b demonstrates the complete solid element mesh including foam, concrete and rigid ground. Solid elements are generated in most cases by following the same mesh pattern of the steel skins and projected with four layers to its third direction. Fig. 9c is a schematic finite element model in colour-filled form to provide physical feeling for the entire system. Basically, the impact region is modelled by a refined mesh at impact area. The refinement is gradually reduced for the region farther away from impact location for economy of computing cost. Mesh details are available in the next section along with presentation of analytical results for each structural component. All contact interfaces among the components of target pad, impact limiter No. 1, the lid, container and impact limiter No. 2 have been considered.

5. ANALYTICAL RESULTS AND DISCUSSION OF IMPACT RESPONSES

The analysis is carried out using the hydrodynamic code DYNA3D(Ref. 6). The analytical data is then fed back to MSC/PATRAN for post-processing. With its colour graphic capability, MSC/PATRAN sorts, interprets, and summarizes the resulting data in suitable forms for presentation.

5.1 Response of the Overall System

In view of the overall response of the entire system, Figs. 10 and 11 are respectively the kinetic energy and the normalized momentum time histories of the container system during the course of impact. Both figures identify the full stop of the container at approximately 0.095 seconds after initial contact and a rebound thereafter. The smoothness of these curves implies a stable numerical analysis being

experienced. Fig. 12 is the time history of the total contact force between impact limiter No. 1 and the rigid target pad throughout the entire impact course. It is seen that the maximum of approximately 20.5 x 10^6 Newtons (about 26.5 g) occurs at approximately 0.084 seconds. Fig. 13 presents a series of system deformation plots at a 0.02 second time interval to provide an equivalent animation. Obviously, the most critical damage occurs at the impact limiter No. 1 and its severeness will be examined closely later.

5.2 Response of Individual Components

For clarity, components of the system (namely: impact limiter No. 1, the lid, the container itself and impact limiter No. 2) are presented separately for their stress, strain and deformation. Each component is further divided into two parts representing different materials (i.e. liner steel/stainless steel and concrete/foam). Stress and strain distribution are plotted on the deformed component so that stress/strain and deformation can be studied simultaneously. For the cases of nonmetallic material (concrete and rigid foam) where tensile strength is significantly less than the compressive strength, hydrostatic pressure is supplemented to report the normal stress state of the material.

5.2.1 Impact Limiter

The peak von Mises stress in the impact limiter No. 1 stainless steel skin is recorded at 0.08 second and three sequential views of bottom, front and top are provided as shown in Fig. 14. It is noticed that the top and inner stainless steel skin hold the rigid polyurethane foam effectively with significantly less deformation when compared to that of the bottom portion of the limiter. It is also interesting to observe that the outer skin is buckled with double folds which is consistent with the experiments of different shaped container previously tested in Ontario Hydro. Highest stress occurs at the tip of the folds as expected where the steel plate experienced the largest stretching and curvature change. It is also noted that stress at inner skin is significantly less than that of outer skin (about one half). However, both outer and inner skin around the impact region (approximately one-quarter of the entire impact limiter) has yielded.

The accumulated total plastic strain in the stainless steel skin is illustrated by a top view at 0.08 second and a bottom view at 0.10 second in Fig. 15. The analysis indicates that there is no further permanent damage after 0.08 second as the entire container system is experiencing elastic unloading thereafter. The maximum strain of 33% at outer skin and approximately 5% at inner skin are well within its ductility limit (see Fig. 4) and hence no ductile fracture failure would be expected.

Von Mises stress distribution in the rigid polyurethane foam with a top and bottom view at 0.08 second is reported in Fig. 16. Higher stress at the inner face of foam occurs at the location corresponding to the corners of the container and is due to container/impact limiter interface contact during impact.

The normal stresses in the foam are demonstrated in terms of hydrostatic pressure in Fig. 17 with two separate views for the inner and outer parts of the foam at 0.08 second and 0.10 second respectively. The pressure (note that the negative value indicates compressive stress) at outer face of the foam is obviously due to impact to the rigid ground while that at inner face is due to contact with the container. The figures demonstrate that the area under direct contact is subjected to compressive stress with the highest stress at the tip as it should be. The rest of the foam has its compressive stress gradually reduced to zero or even tensile due to elastic lateral expansion of the material body.

Stress and strain in the impact limiter No. 2 are very small and hence not presented.

5.2.2 Container

The von Mises stress distribution in the cover plates of the lid is shown in Fig. 18 and is below the employed yield strength of 370 MPa. It is interesting to note that the higher stresses arrive at one corner earlier than the other corner. This is due to nonsymmetry of the structure (compare the dimension 2.418m against 2.110m in Fig. 1) which causes the container to contact impact limiter at one corner earlier than the other. Furthermore, the vertical plate at the side of 2.418m possesses a larger aspect ratio than the plate at the other side of 2.110m and hence is more flexible (weaker). It therefore tends to yield first and then has the stress redistributed to the other side.

Fig. 19 presents the accumulated plastic strain in the lid plate at 0.10 second. It is seen that the lid plate only experiences a very small amount of plastic strain (about 2%) at a small localized area. The majority of the lid remains elastic throughout the entire course of impact.

The response of the lid concrete follows the similar pattern of steel plate. Von Mises stress distribution at 0.10 second is shown in Fig. 20. The accumulated plastic strain is illustrated in Fig. 21 which identifies the location and size of concrete being failed. Fig. 22 demonstrates the magnitude of hydrostatic pressure in concrete.

The highest von Mises stress in the container outer liner is shown in Fig. 23 at 0.08 second. The stress remains at a relatively low level. Stress in the inner liner is even less significant. Because the entire liner remains elastic throughout the impact course, no plastic strain is recorded.

Stress in the container concrete is selectively shown in Fig. 24 and also remains at a relatively low level. The only recorded plastic strain in the concrete is an extreme small amount with no physical significance. Practically the container responds elastically throughout the impact. The hydrostatic pressure in the concrete is presented in Fig. 25 (at 0.08 second).

6. CONCLUSION

An impact analysis of a concrete storage container using MSC/PATRAN for pre- and post-processing has been illustrated. MSC/PATRAN enables the response of the container system in terms of various parameters at different stages of impact to be studied in details. The information obtained is very useful for container design.

It is found that damage tends to localize in the vicinity of contact with stresses and strains decreasing rapidly toward remote areas. An impact limiter composed of stainless steel skin and filled with efficient energy absorption material such as rigid polyurethane foam can arrest the impact on the container effectively. Even though the impact limiter experiences severe damage, damage on the container itself is not observed as it remains essentially elastic.

REFERENCES

(1) Conway, J.B., Stentz, R.H. and Berling, J.T., Fatigue, Tensile and Relaxation Behaviour of Stainless Steels, TID-26135, Technical Information Centre, Office of Information Services, United States Atomic Energy Commission, 1975.

(2) Sato, J. and Andre, H., Concrete Integrated Container (CIC) Program, Construction of 1/4 and 1/8 Scale Models, Ontario Hydro Research Division Report 88-97-K, 1988.

(3) Chen, W.F., Plasticity in Reinforced Concrete, McGraw-Hill, 1982.

(4) Traeger, R.K., Physical Properties of Rigid Polyurethane Foams, Journal of Cellular plastics, 9, 405, 1967.
(5) MSC/PATRAN User Manual, Version 2.5, The MacNeal-Schwendler Corporation, California, U.S.A., 1988
(6) Sauve, R.G., Ontario Hydro DYNA3D Computer Code System VAX/VMS Version, Ontario Hydro Report No. 87-222, 1987.

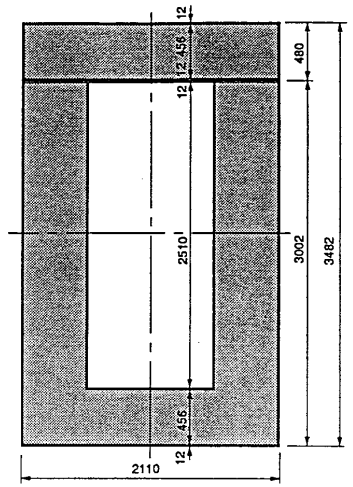

(a) Section View

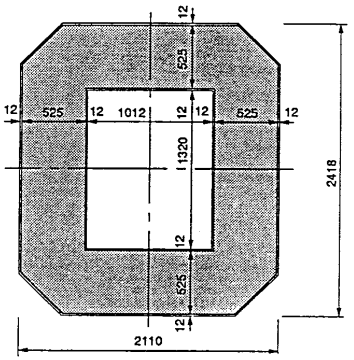

(b) Plane View

FIG. 1. Configuration of the container

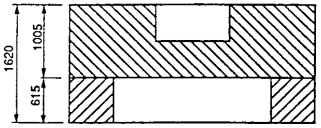

Section View (limiter No.2)

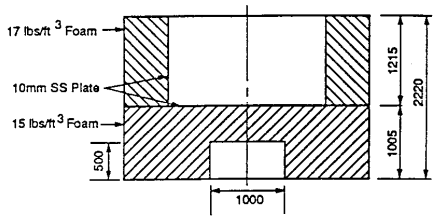

Section View (limiter No.1)

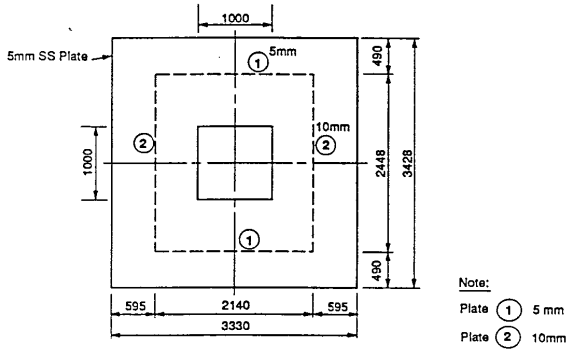

Plane View

FIG. 2. Configuration of impact limiter

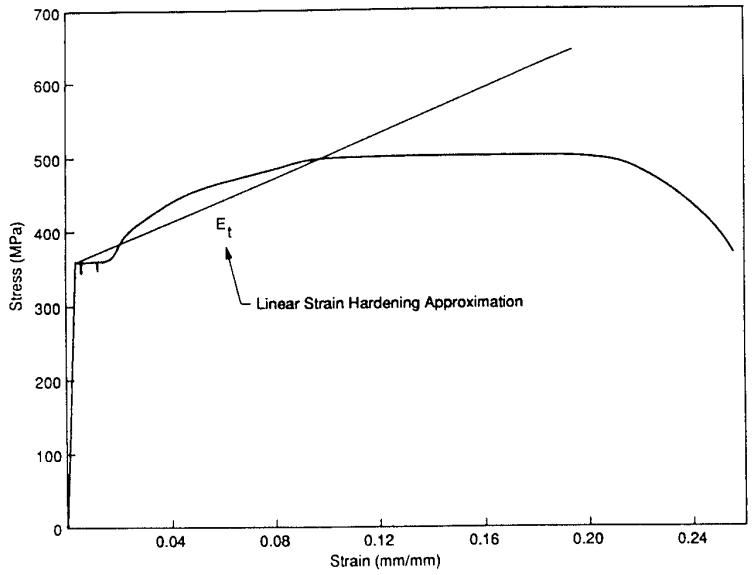

FIG. 3. Stress-strain curve of steel liner

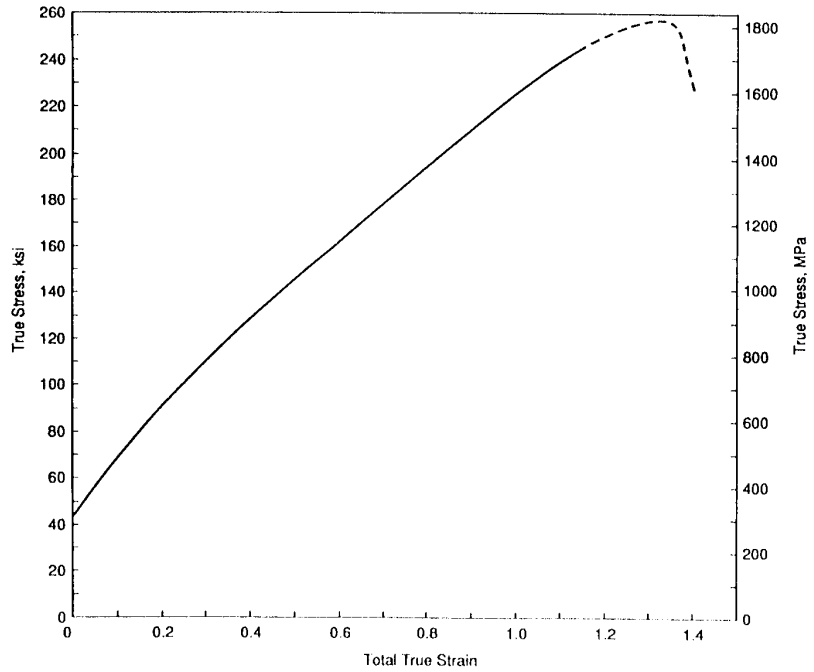

FIG. 4. Stress-strain curve of stainless steel

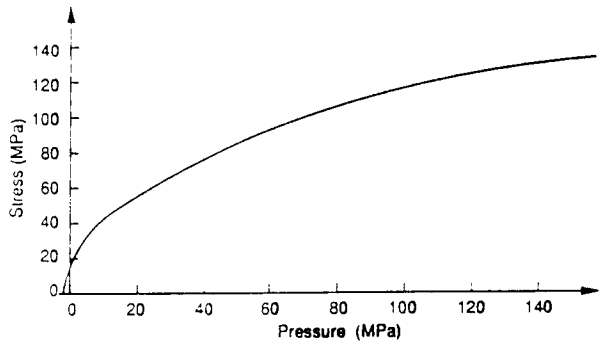

FIG. 5. Yield stress - pressure relation of concrete

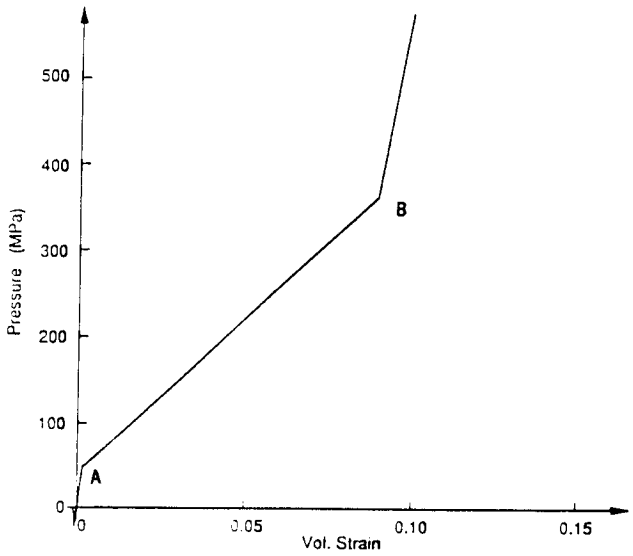

FIG. 6. Equation of state model of concrete

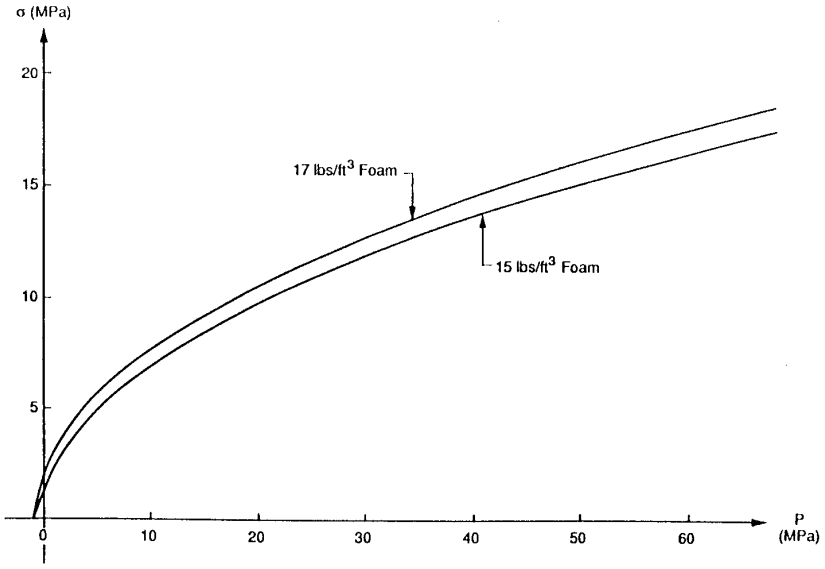

FIG. 7. Yield stress - pressure relation of foams

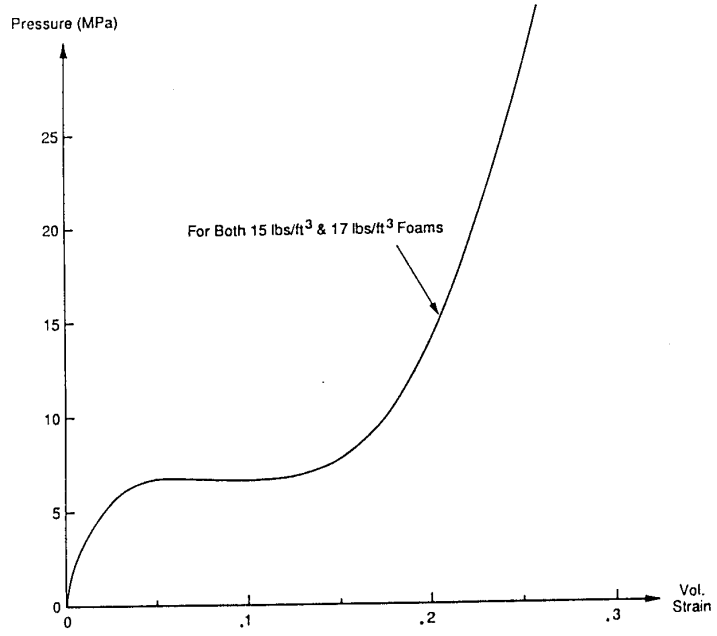

FIG. 8. Equation of state model of foams

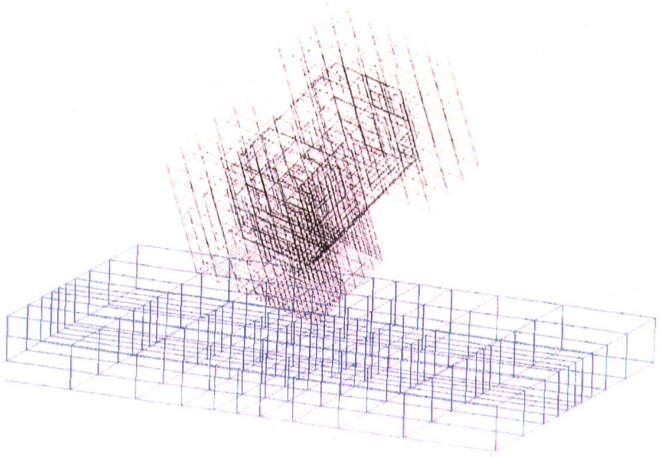

(a) Shell elements for steel plates

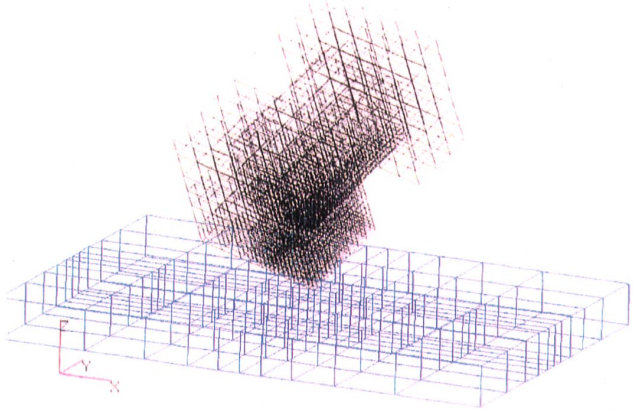

(b) Solid elements for concrete and polyurethane foam

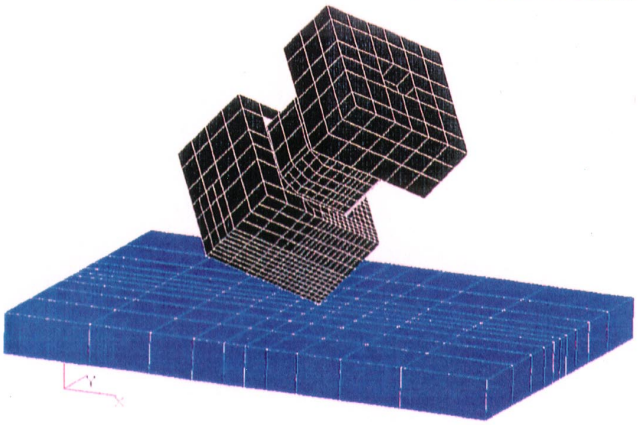

(c) Color filled perspective view

FIG. 9. Finite element model of the container system

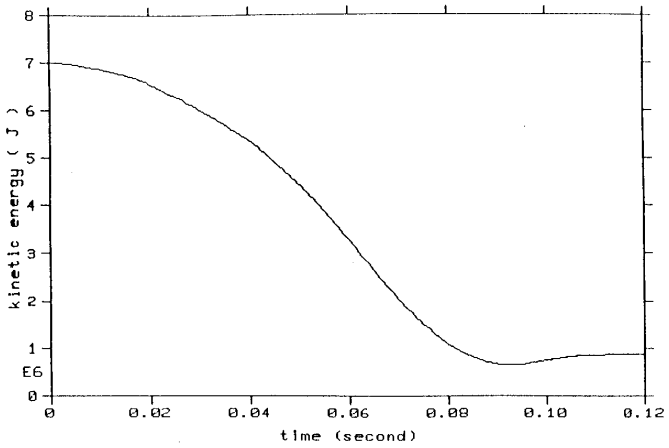

FIG. 10. Kinetic energy time history of the container system

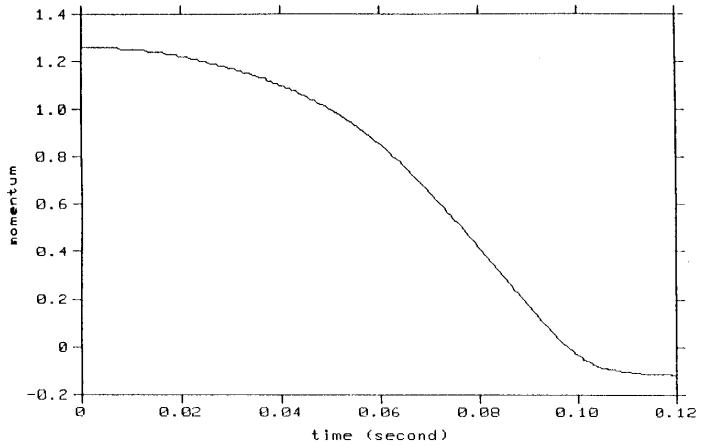

FIG. 11. Normalized momentum time history of the container system

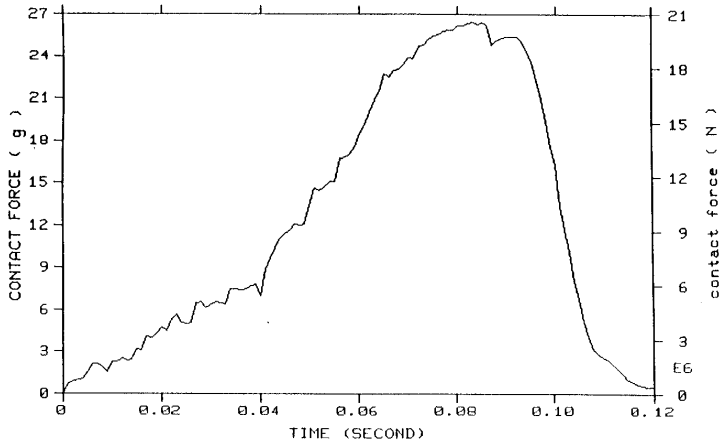

FIG. 12. Contact force time history of the container system

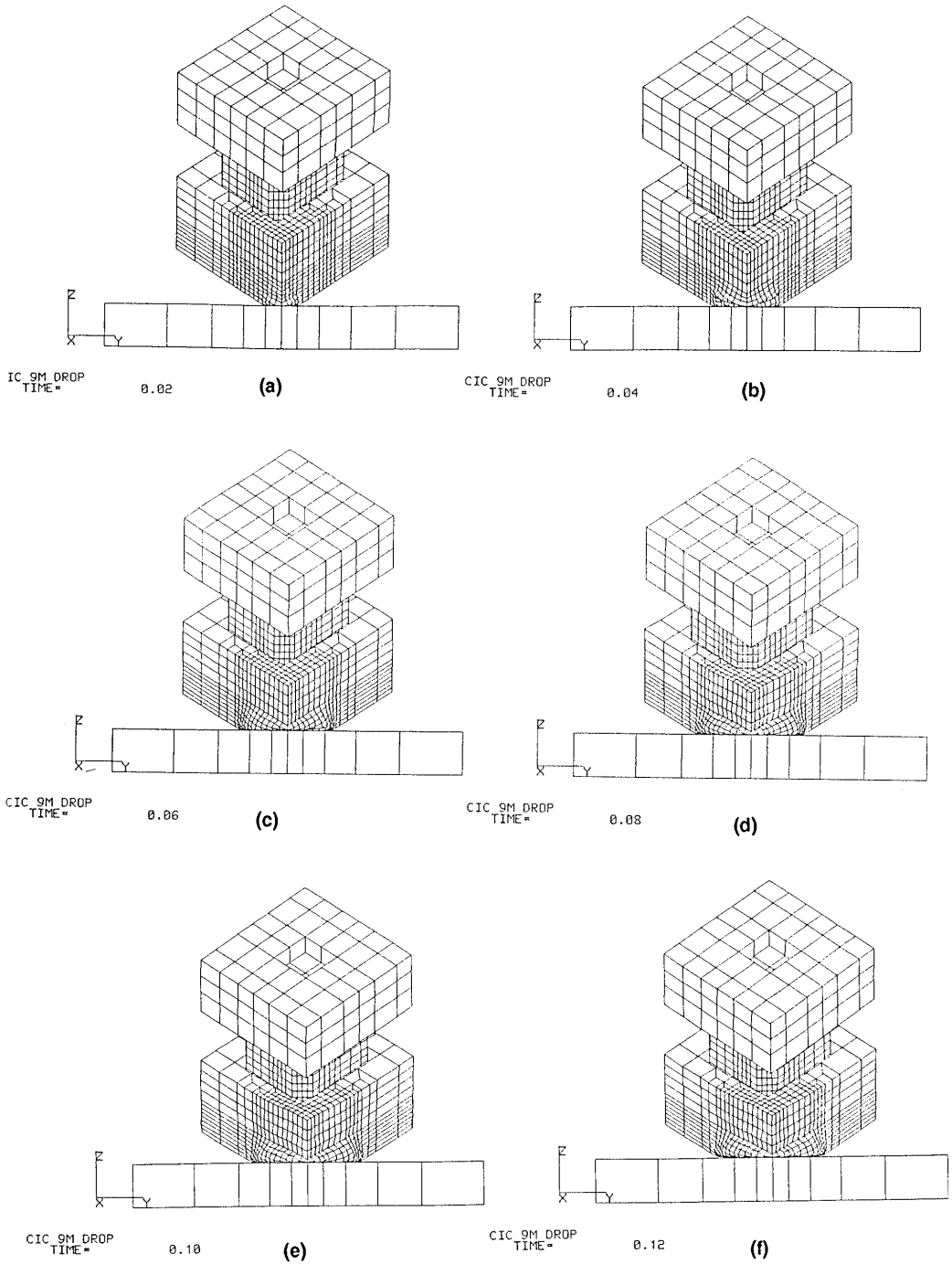

FIG. 13. Sequential deformation of the container system

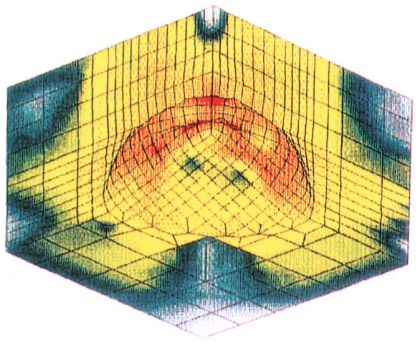

(a) Bottom view

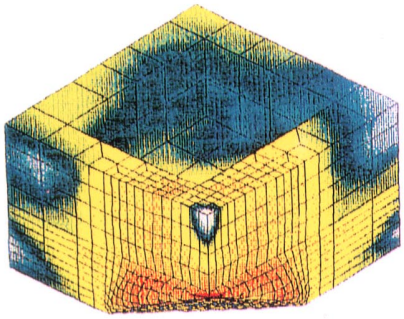

(b) Front view

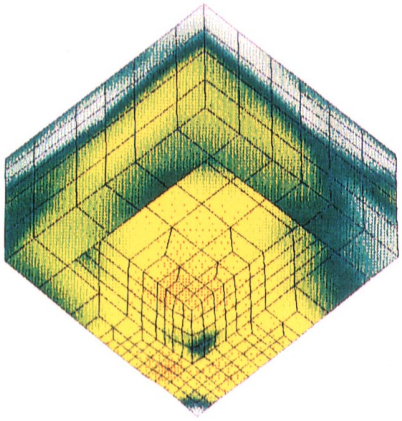

(c) Top view

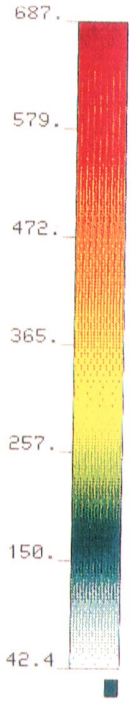

FIG. 14. von Mises stress in the stainless steel skin of the impact limiter no. 1 at 0.08 second (MPa)

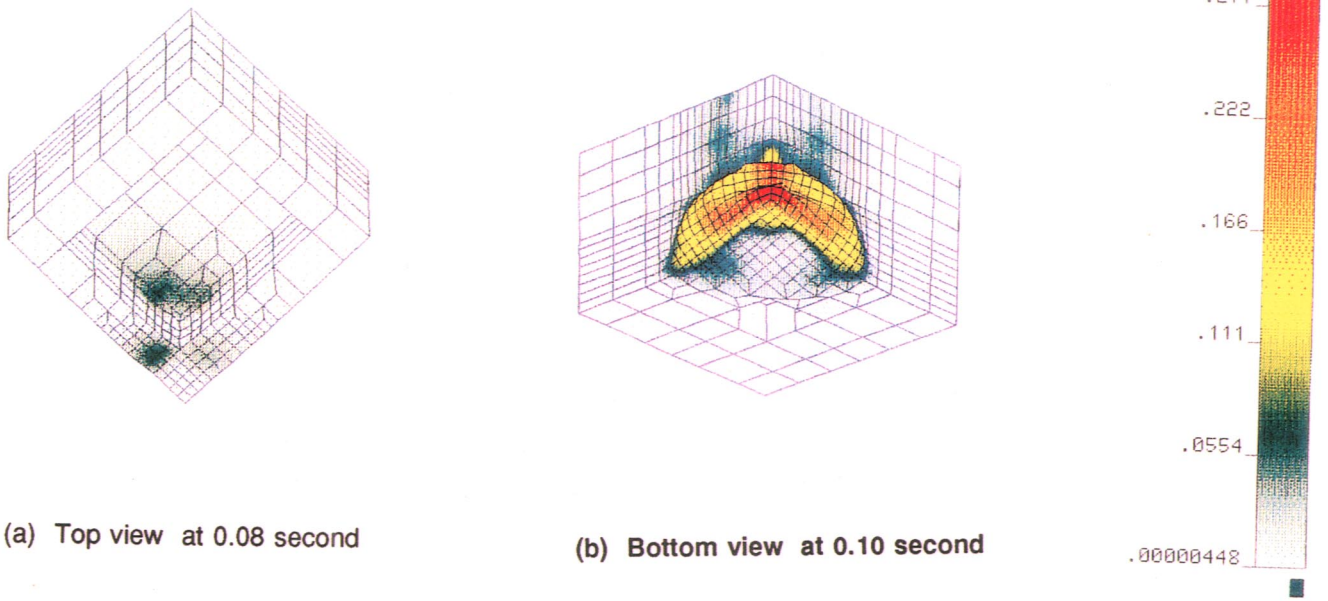

(a) Top view at 0.08 second

(b) Bottom view at 0.10 second

FIG. 15. Accumulated equivalent plastic strain in the stainless steel skin of the impact limiter no.1

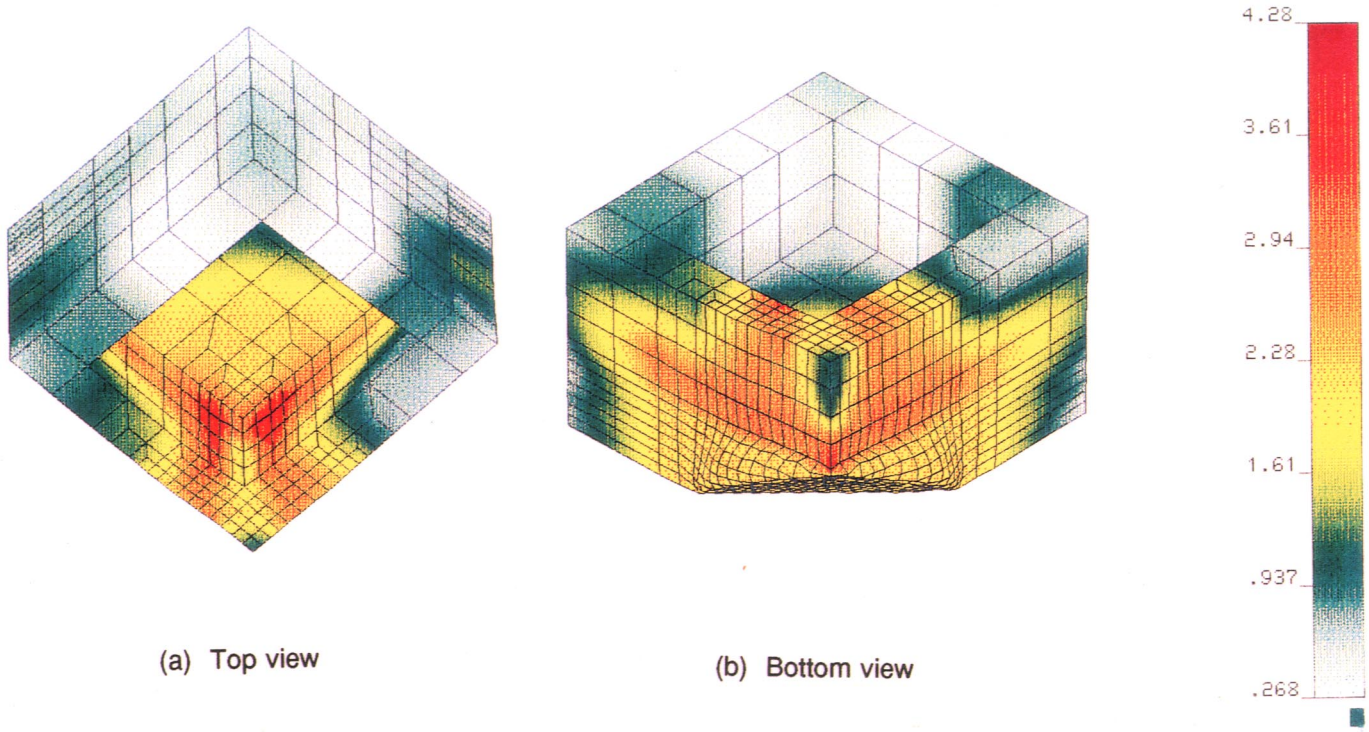

(a) Top view

(b) Bottom view

FIG. 16. von Mises stress in the polyurethane foam of the impact limiter no. 1 at 0.08 second (MPa)

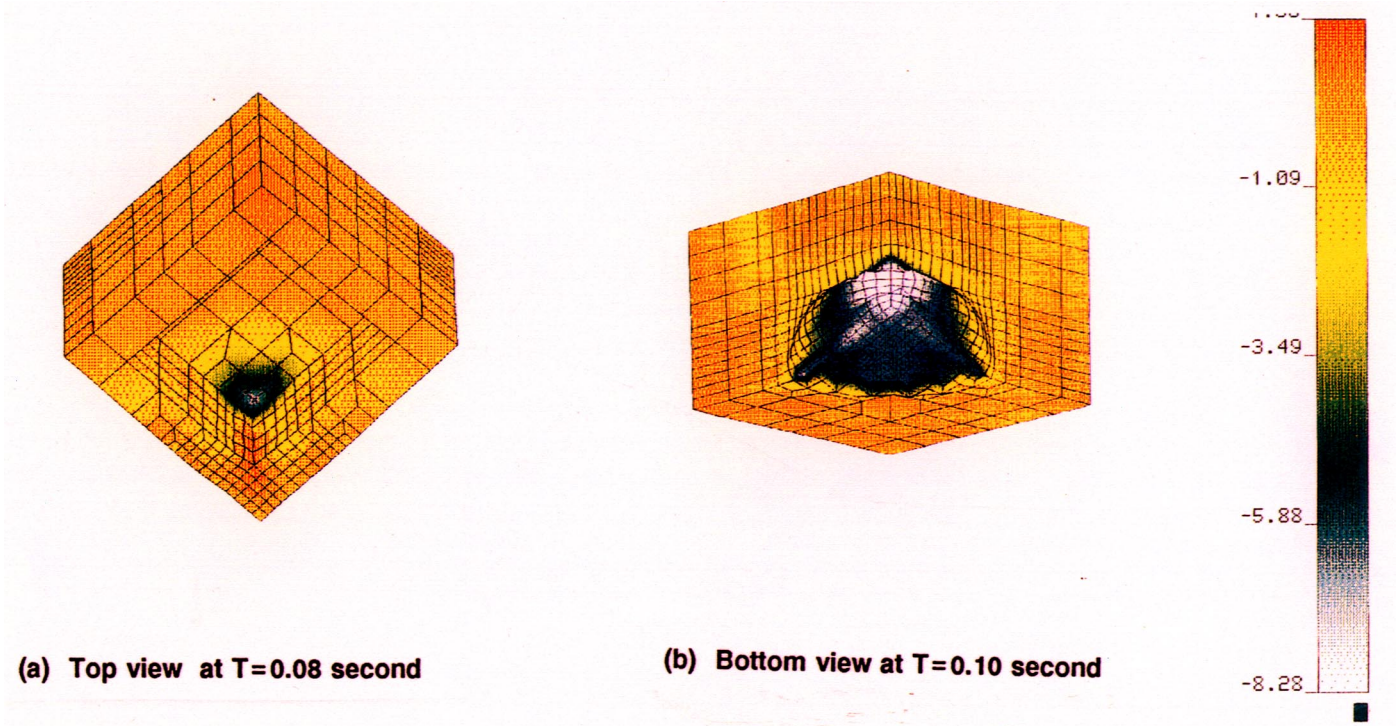

(a) Top view at T=0.08 second

(b) Bottom view at T=0.10 second

FIG. 17. Hydro static pressure in foam - Impact limiter No. 1

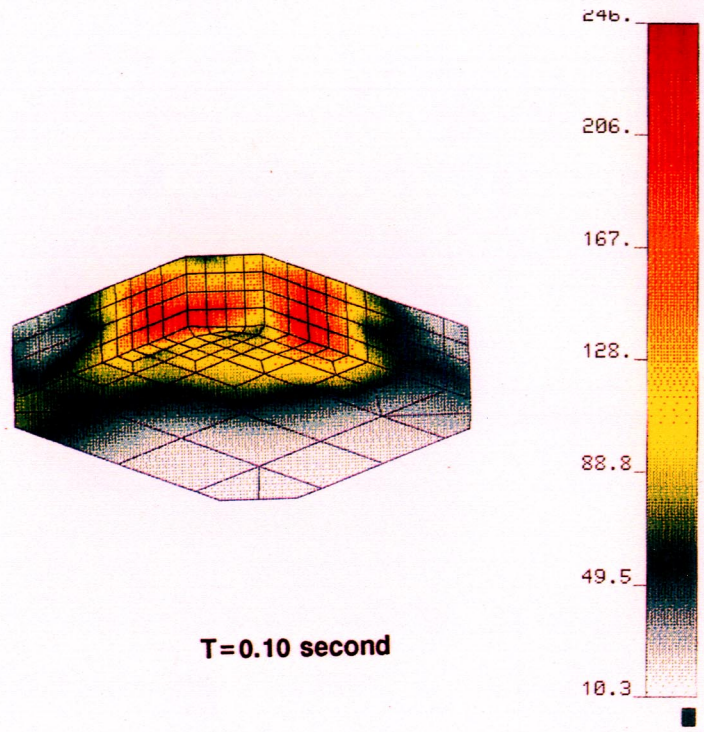

FIG. 18. von Mises stress in lid steel plate(MPa)

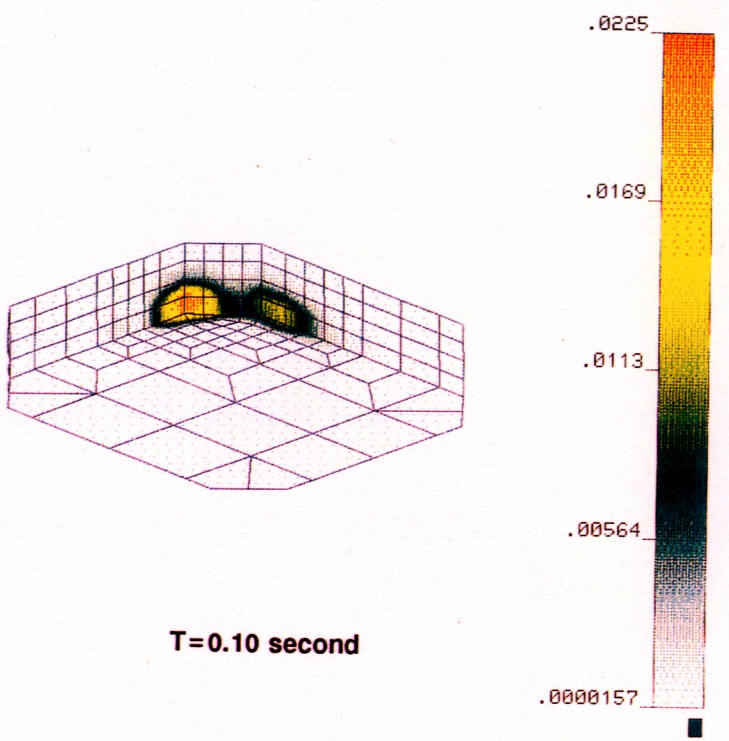

FIG. 19. Plastic strain in lid steel plate

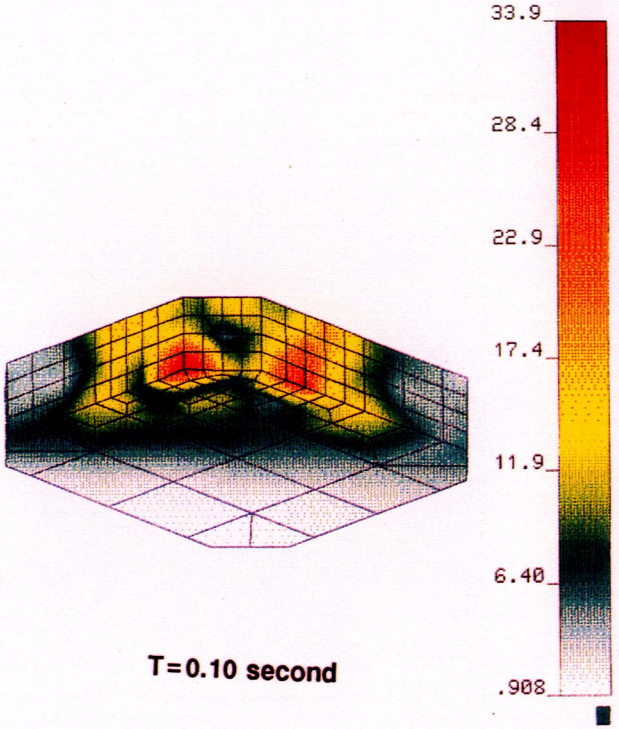

T=0.10 second

FIG. 20.

von Mises stress in lid concrete(MPa)

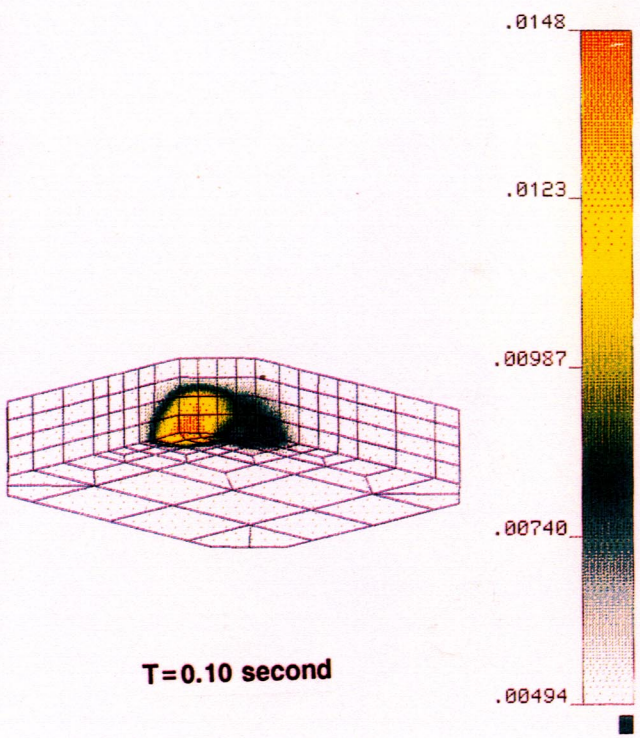

T=0.10 second

FIG. 21.

Plastic strain in lid concrete

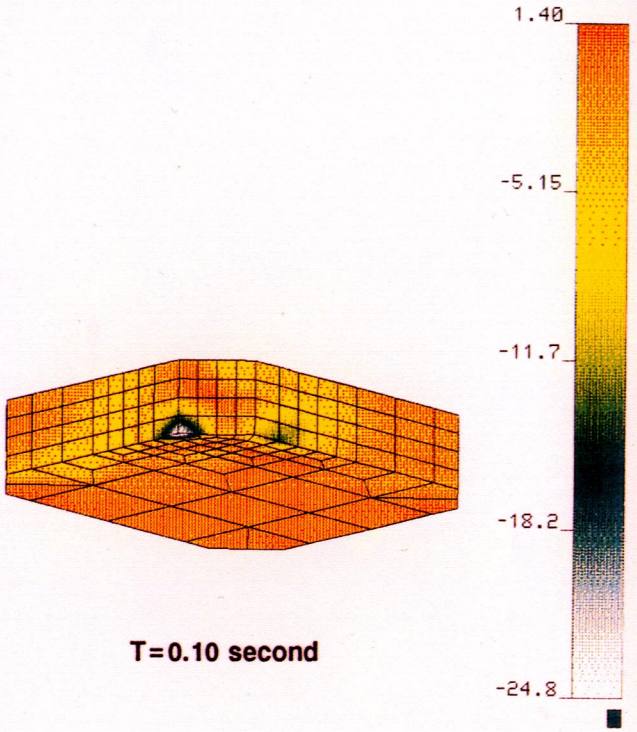

T=0.10 second

FIG. 22.

Hydro static pressure in lid concrete(MPa)

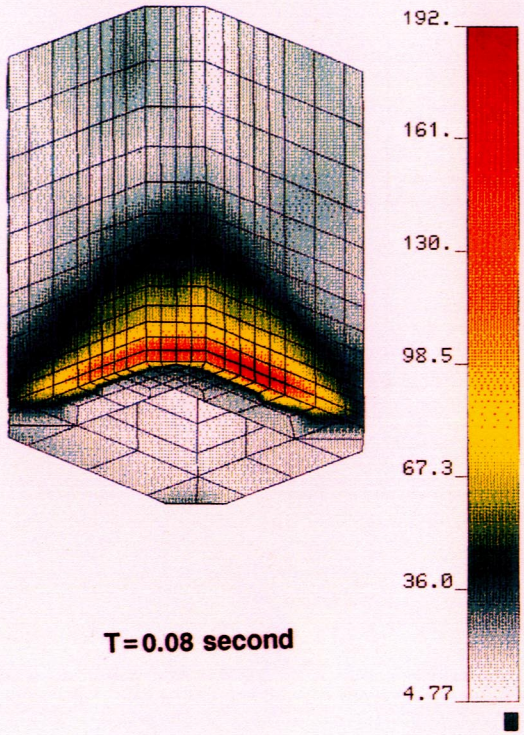

T=0.08 second

FIG. 23.

von Mises stress in container steel liner(MPa)

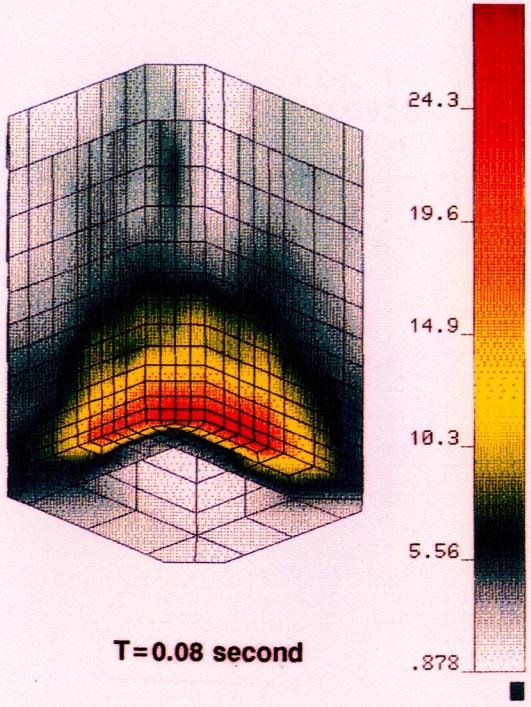

T=0.08 second

FIG. 24.

von Mises stress in container concrete(MPa)

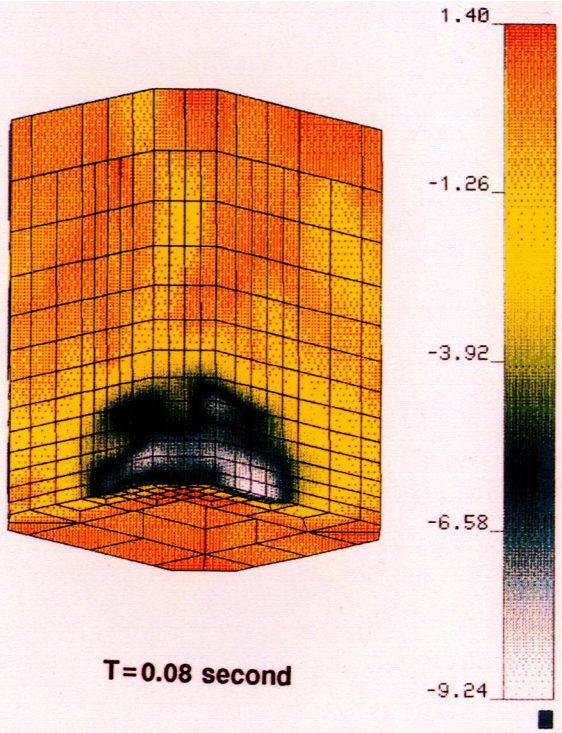

T=0.08 second

FIG. 25.

Hydro static pressure in container concrete(MPa)